arXiv:1304.3900v1 [cond-mat.soft] 14 Apr 2013

Depth resolved grazing incidence scattering from the solid-liquid interface

Max Wolff, Peter Kuhns, Andrew J. C. Dennison
Department of Physics and Astronomy, Uppsala University, 75121 Uppsala, Sweden

E-mail: `max.wolff@physics.uu.se`

Georg Liesche, Philipp Gutfreund
Institut Laue-Langevin, 38042 Grenoble, France

Sarah Rogers
ISIS-STFC, Rutherford Appleton Laboratory, Chilton, Oxon OX11 0QX, United Kingdom

Abstract. We have applied small angle scattering in grazing incidence beam geometry on a time-of-flight neutron instrument. Due to the broad wavelength distribution provided for a specific incident beam angle the penetration depth of the neutron beam is varied over a broad range in a single measurement. The near surface structure of polymer micelles close to silicon substrates with distinct surface energy is resolved. It is observed that the very near-surface structure strongly depends on the surface coating whereas further away from the surface bulk like ordering is found. A more pronounced ordering is found close to surfaces with high surface energy.

1. Introduction

Due to the self-assembling property on the molecular scale, block polymers are one promising way for the fabrication of nano-devices [1, 2]. In particular, close to a solid boundary one expects surface enrichment in case of an attractive interaction between the interface and one of the building blocks, or depletion in case of a repulsive interaction. This may lead to lamellar phases with different orientations with respect to the interface [3].

In aqueous solution block polymers may form micelles since the hydrophobicity of the building blocks may repel water molecules. As the properties of different blocks may change with e.g. temperature or pressure, block polymers offer a model system for the study of gelation, percolation, crystallization or the glass transition [4]. Previously, the ordering of micelles at the solid-liquid interface was studied by off-specular neutron scattering [5]. Grazing incidence small angle neutron scattering (GISANS) expands on this technique by offering resolution for the scattering in all three dimensions [6] thus providing a unique insight into the interfacial structure.

Following along this line recent developments in instrumentation have provided an

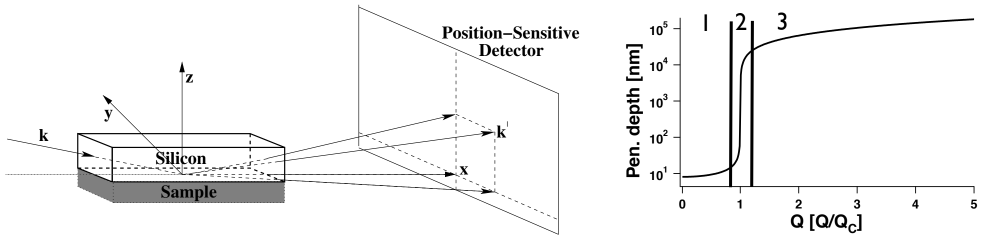

Figure 1. Schematics of the scattering geometry used for grazing incidence neutron scattering at the solid-liquid interface (left panel) [6]. The right panel depicts the penetration depth of the neutron beam plotted over the transfer of momentum, normalized to the critical transfer of momentum for total external reflection. The regions 1, 2 and 3 mark the Q intervals at which the GISANS data were taken.

optimized beam geometry and flux for GISANS studies [7, 8]. In this context experiments showed that the signal from the bulk of a sample might be separated from the surface scattering [9] or that time-of-flight TOF-GISANS can be used to probe a large range of momentum transfers for a single incident beam angle [10, 11]. In this proceeding we describe a scattering experiment probing the near surface structure of a micellar polymer solution, which is in its cubic (fcc) phase. We demonstrate that by combining a broad neutron wavelength spectrum with a grazing incidence beam geometry on a TOF-SANS instrument, the structure of the polymer micelles can be resolved close to the solid surface as well as in the bulk in one single measurement.

2. Experimental details

Two functionalized single crystalline silicon (100) substrates (70*70*10 mm^3, polished, obtained from CrysTec, Germany) were used as solid interface. One wafer was chemically cleaned in freshly prepared piranha acid (50/50 v/v H_2SO_4 (concentrated) and H_2O_2 (30 % aqueous)) for 30 minutes and rinsed with Millipore water. This procedure leads to an interfacial energy of approx. $\gamma = 34.35 \frac{mJ}{m^2}$ at room temperature [12, 13]. The second wafer was cleaned in the same way and subsequently chemically covered with a self-assembled monolayer of octadecyltrichlorosilane OTS. The resulting interfacial energy is about $\gamma = 7.2 \frac{mJ}{m^2}$ at room temperature [13].
The sample is a 18.5 % (in weight, corresponding to 20 % in H_2O) solution of Pluronic F127 ((ethylene oxide)$_{99}$-(propylene oxide)$_{65}$-(ethylene oxide)$_{99}$) in deuterated water. The bulk properties of this material have been reported in literature in great detail [14, 15]. The polymer was purchased from Sigma-Aldrich and used without further purification. The molecules were solved in deuterated water (for better contrast) at a low temperature under constant stirring until a homogeneous solution was formed. The sample cell was then filled with the sample in its liquid state at 5 °C.
Figure 1 (left panel) depicts the scattering geometry for the neutron scattering experiments. Neutrons penetrate a single crystalline block of silicon from the narrow side and get scattered at the solid-liquid interface. A detailed discussion of the scattering geometry can be found in [16]. The TOF-GISANS experiments were done on the instrument SANS-2D at ISIS (Rutherford Institute, Didcot, England). In order

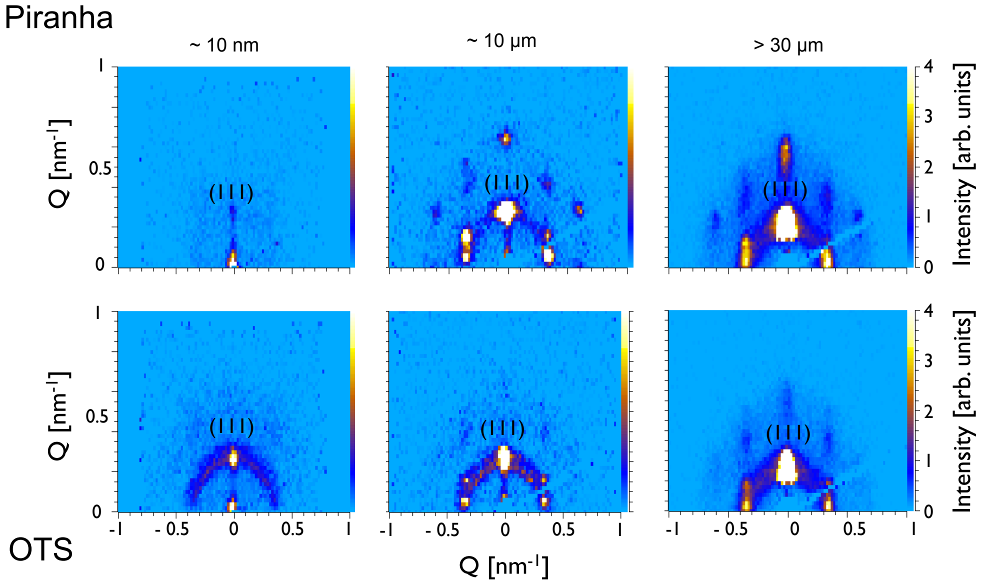

Figure 2. GISANS data taken for a 18.5 % (in weight) solution of the polymer F127 solved in deuterated water in contact with a silicon surface treated with piranha acid (top panels) and OTS (lower panels). The different penetration depths, noted at top and increasing from left to right, result from the different wavelengths in the incoming beam. The crystalline ordering is clearly preferred in the vicinity of the piranha acid treated treated surface.

to probe different penetration depths the intensities were integrated for one incident beam angle over wavelength intervals of 1.75-5 Å, 5-6 Å, 6-15.6 Å, corresponding to wavelength resolutions of $\frac{\Delta\lambda}{\lambda}$ of 48 %, 9 % and 44%, respectively. The incident beam was collimated over a distance of 6 m. The source slit was set to a width and height of 20 mm and 4 mm and the sample slit to 10 mm and 0.2 mm, resulting in a beam divergence of 0.29° and 0.04°, respectively. The incident beam angle was chosen to be 0.3° resulting in a critical wavelength for total external reflection of $\lambda_c = 5.4$ Å.

3. Results and discussion

Figure 2 depicts the patterns of intensity measured on SANS-2D for a 18.5 % (in weight) solution of the polymer F127 solved in deuterated water. The three pictures for the silicon surface treated with piranha acid (top panels) and OTS (lower panels) were taken simultaneously for one incident beam angle with a fixed detector angle. The left panels correspond to the integration of the detector images for wavelengths ranging from 6-15.6 Å resulting in a penetration depth of the neutron beam into the polymer solution of approximately 10 nm (region 1 in Figure 1). The intensity integrated for short wavelengths of 1.75-5 Å and thus a large penetration depth of about 30 μm is depicted in the right panels. The central column summarizes the intensities for wavelengths integrated around the critical wavelength, 5-6 Å, resulting in an intermediate penetration depth of about 10 μm.

For the smallest penetration depth of about 10 nm a ring of scattered intensity is

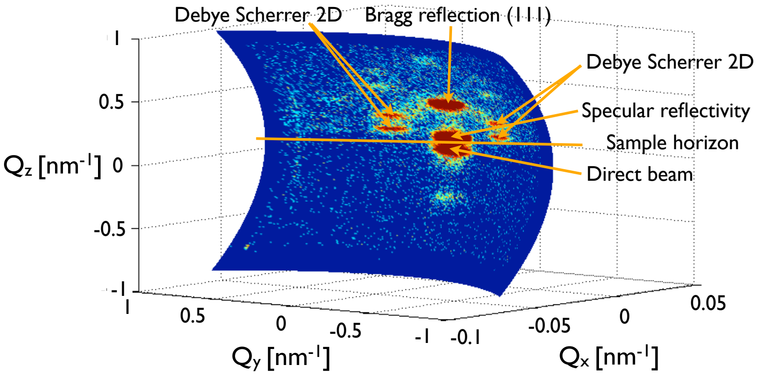

Figure 3. Detector image for a fcc crystalline structure plotted as color map on a surface spanned in Q space. The logarithm of high and low intensity is represented by the red and blue color, respectively,

visible around the direct beam (Q=0) for the OTS substrate. This ring is absent for the micelles in contact with the surface treated with piranha acid. The difference in the intensity distribution for the sample in contact to the two solid substrates becomes more clear for larger penetration depths (middle panels). At least ten Bragg reflections can be clearly distinguished with the sample in contact to the piranha acid treated surface, whereas still the ring of scattered intensity is dominant for the OTS. For the largest penetration depth (right panels) both detector images become more similar. For the piranha acid treated surface the diffuse scattering becomes increased, whereas for the OTS one the reflections are separated more clearly.

In order to understand the crystalline structure formed at the different distances from the solid substrate and to relate those to the scattering patterns presented in Figure 2 it is important to have a closer look on the scattering geometry and how the instrumental settings probe the reciprocal lattice of the crystal. Figure 3 depicts intensities for the same kind of cubic structure formed by F127 micelles solved in deuterated water taken on the instrument ADAM at the Institute Laue-Langevin (Grenoble, France) [17]. This instrument uses a monochromatic neutron beam of 4.41 Å. The incident beam was collimated in order to well resolve the Bragg reflections. In Figure 3 the logarithm of the scattered intensity is plotted as a color map (high and low intensity in red and blue, respectively) on a surface spanned in Q space over all three coordinates Q_x, Q_y and Q_z. The coordinate system x, y and z is defined with respect to the sample surface as shown in Figure 1. A more detailed discussion of the length-scales probed along the different directions can be found in [18]. It is clear that the detector plane represents a curved surface with Q=0 at the position of the direct beam. The second and only other point where the in-plane coordinates Q_x and Q_y are zero is the point where the specular scattered intensity is detected. All other points on the detector have none zero Q_x and/or Q_y components.

Considering a densely packed cubic structure at the interface, the (111) lattice planes would be parallel to the solid-liquid boundary and the Bragg reflections resulting from them should have no in-plane component ($Q_x = Q_y = 0$). This implies that the (111) reflection can only be detected if it has a certain Rocking width along Q_x. The values probed along the Q_x direction are much smaller than those probed along Q_y and Q_z

and for a crystal coherence on the order of μm a finite intensity is detected in the detector plane. Moreover with decreasing wavelength the momentum transfer along the x direction decreases at the position of the Bragg refelection for small Q [16]. This implies that for a specific crystal coherence the intensity scattered into the detector plane should increase with decreasing wavelength. All other four Bragg reflections are only visible if the crystalline structure has a two dimensional powder structure with respect to the sample interface [18].

Considering the scattering geometry the intensity distribution visible in Figure 2 can be understood. Our model bases on a larger coherence of the crystal and better epitaxy close to the surface cleaned with piranha acid. For the smallest penetration depth (left panels) and the largest wavelength a relatively large Q_x is probed. Considering the large coherence of the crystal it becomes clear why almost no intensity is visible in the upper left panel. On the other hand for the more powder like structure with small coherence close to the OTS surface the ring of intensity visible in the lower panel on the left hand side becomes understandable. With decreasing wavelength and increasing penetration depth the component of Q_x at the Bragg peak becomes smaller. The good crystallinity next to the piranha acid cleaned surface is well reflected in the hugely increasing intensity of the (111) reflection and the large number of visible reflections in this case. For the OTS interface the intensity increases less and a lot of diffuse scattering is visible. For the largest penetration depth (right panels) the two scattering patterns, top and bottom, become more similar resembling a more bulk like ordering in the sample. In addition all reflections become more smeared out since the intensity is integrated over a large wavelength band.

Due to refractive effects a correction with respect to the refractive index should be applied for Q values close to the sample horizon. Since the Bragg reflections under discussion here are at Q values at least three times larger than the critical momentum of total external reflection this corrections are negligible and the kinematic approximation can be used.

4. Conclusion

In this proceeding we present a TOF-GISANS experiment to resolve the near surface structure of micellar systems. By use of TOF neutron reflectometry and small angle scattering depth sensitive information is extracted. It turns out that with increasing distance from the interface the crystallographic structure approaches the bulk structure. Our experiments open new possibilities for the investigation of near-surface structures over several orders in length scale not only of micellar systems but also of colloids.

5. Acknowledgement

The authors thank Katharina Theis-Bröhl for sending Georg Liesche for a project work to the Institute Laue-Langevin and acknowledge financial support by the Swedish research council VR under contract number A0505501, as well as the European Union NMI-3 initiative for financial assistance for travel. We acknowledge STFC for the beam time, RB1120261.

References

[1] S. Ludwigs, A. Boker, A. Voronov et al. 2003 *Nature materials* **2** 744.

[2] S.O. Kim, H.H. Solak, M.P. Stoykovich et al. 2003 *Nature* **424** 411.

[3] E. Huang, T.P. Russell, C. Harrison et al. 1998 *Macromolecules* **31** 7641.

[4] W.-R. Chen, S.-H. Chen, F. Mallamace 2002 *Phys. Rev. E* **66** 021403.

[5] D.J. McGillivray, R.K. Thomas, A.R. Rennie et al. 2003 *Langmuir* **19** 7719.

[6] M. Wolff, U. Scholz, R. Hock, A. Magerl and H. Zabel 2004 *Phys. Rev. Lett.* **92** 255501.

[7] Chaboussant G., D esert S., Lavie P., Brulet A. 2012 *Journal of Physics: Conference Series* **340** 012002.

[8] Mitamura K., Yamada N., Sagehashi H., Seto H., Torikai N., Sugita T., Furusaka M., Takahara M. 2011 *Journal of Physics: Conference Series* **272** 012017.

[9] Cousin F., Jestin J., Chaboussant G., Gautrot S., Menelle A., Ott F. 2009 *Eur. Phys. J. Special Topics* **167** 177183.

[10] Kaune G., Haese-Seiller M., Kampmann R., Moulin J.-F., Zhong Q., Müller-Buschbaum P. 2010 *Journal of Polymer Science: Part B: Polymer Physics* **48** 16281635.

[11] Müller-Buschbaum P., Metwalli E., Moulin J.-F., Kudryashov V., Haese-Seiller M., Kampmann R. 2009 *Eur. Phys. J. Special Topics* **167** 107112.

[12] Maccarini, M.; Steitz, R.; Himmelhaus, M.; Fick, J.; Tatur, S.; Wolff, M.; Grunze, M.; Janecek, J.; Netz, R. R. 2007 *Langmuir* **23** 598608.

[13] P. Gutfreund, M. Wolff, M. Maccarini, S. Gerth, J. F. Ankner, J. Browning et al. 2011 *J. Phys. Chem* **134** 64711.

[14] Mortensen, K. 2001 *Polym. Adv. Technol.* **12** 2.

[15] Mortensen, K.; Batsberg, W.; Hvidt, S. 2008 *Macromolecules* **41** 1720.

[16] M. Wolff, A. Magerl and H. Zabel 2005 *Euro. Phys. J. E* **16(2)** 141.

[17] M. Wolff, K. Zhernenkov, H. Zabel 2007 *Thin solid films* **515** 5712.

[18] M. Wolff, A. Magerl, H. Zabel 2009 *Langmuir (Letter)* **25 (1)** 64.